Effects of ^{6}Li excitation in ^{64}Zn($\vec{d}$,^{6}Li)^{60}Ni at low energies

J. E. Bowsher, T. B. Clegg, H. J. Karwowski, E. J. Ludwig, and W. J. Thompson
Department of Physics and Astronomy, University of North Carolina, Chapel Hill, North Carolina 27599 and Triangle Universities Nuclear Laboratory, Durham, North Carolina 27706

J. A. Tostevin
Department of Physics, University of Surrey, Guildford, Surrey, England
(Received 16 October 1991)

Cross sections and the analyzing powers A_y, A_{yy}, and A_{xx} for the ^{64}Zn(d,^{6}Li)^{60}Ni reaction forming the ground and first-excited states of ^{60}Ni are measured in 5° steps from $\theta_{lab}=25°$ to 80° using a 16.4-MeV vector- and tensor-polarized deuteron beam. The ^{6}Li ground state and seven other states, each representing ^{6}Li continuum states of a given spin and internal orbital angular momentum, are included in finite-range, coupled-channel Born approximation (CCBA) calculations for ^{64}Zn(d,^{6}Li)^{60}Ni. The CCBA calculations demonstrate that α transfers forming these continuum states, particularly those forming the first 3^+ state in ^{6}Li, affect the ^{64}Zn(d,^{6}Li)^{60}Ni cross sections and analyzing powers strongly.

PACS number(s): 25.45.Hi, 24.50.+g, 24.70.+s

I. INTRODUCTION

Transfer reactions initiated by polarized beams serve as useful probes of reaction mechanisms and may lead to improved understanding of nuclear structure and spectroscopy. In this paper we report measurements of the differential cross section $d\sigma/d\Omega$, the vector analyzing power (VAP) A_y and the tensor analyzing powers (TAP) A_{yy} and A_{xx} for the ^{64}Zn(d,^{6}Li) reaction at $E_d=16.4$ MeV leading to the ground and first-excited states of ^{60}Ni. A striking feature of the data for the ^{60}Ni ground-state transition is the predominantly negative VAP. These VAP data are not satisfactorily reproduced by finite-range, distorted-wave Born approximation (DWBA) calculations. However, DWBA calculations and angular momentum matching considerations suggest that transfer through the $l=2, I^\pi=3^+$ state of the $d+\alpha$ system could be a source of such spin selectivity. Consequently we, for the first time, consider the ^{6}Li ground state and seven other wave functions, each representing ^{6}Li continuum states of a given spin, I, and internal orbital angular momentum, l, where $l\leq 2$, in finite-range, coupled-channel Born approximation (CCBA) calculations for the (d,^{6}Li) reaction. Calculations are performed using the computer code FRESCO [1]. Coupling and diagonal channel interactions are generated consistently within a $d+\alpha+^{60}$Ni cluster model. Agreement with the VAP data is not obtained, perhaps because the underlying d-^{60}Ni and α-^{60}Ni interactions are not well determined at these energies or perhaps because additional mechanisms, such as Coulomb breakup, must be considered. However, the CCBA calculations do indicate that, at these energies, transfers forming ^{6}Li continuum states strongly influence (d,^{6}Li) observables.

Also measured and used to constrain the optical potentials employed in the (d,^{6}Li) calculations were angular distributions, in 5° steps from $\theta_{lab}=20°$ to 165°, of $d\sigma/d\Omega$, A_y, A_{yy}, and A_{xx} for ^{64}Zn($\vec{d}$,d)^{64}Zn scattering at $E_d=16.4$ MeV and of $d\sigma/d\Omega$ for ^{60}Ni(^{6}Li,^{6}Li)^{60}Ni scattering at $E_{Li}=14.8$ MeV, the outgoing ^{6}Li energy in ^{64}Zn ($\vec{d}$,^{6}Li)^{60}Ni(g.s.).

In the remainder of the Introduction, we review related previous work on the (d,^{6}Li) reaction. This reaction has been investigated extensively, primarily by cross-section measurements utilizing a wide range of targets and incident beam energies and by one-step, DWBA analyses of these data. These analyses have often focused on extracting target α-particle spectroscopic factors from the data [2–6]. There are, however, significant discrepancies between measured and predicted spectroscopic factors [6]. Other studies have examined the dependence of DWBA calculations on optical model parameters and on the interactions and wave functions describing the bound states of ^{6}Li and the target [2,4,7]. Multistep analyses of the (d,^{6}Li) reaction have been few in number. Palla and Oelert [8] utilized the coupled-reaction-channels formalism to study the effects of couplings to excited states of the target and the residual nucleus for the ^{24,26}Mg(d,^{6}Li)^{20,22}Ne reactions at $E_d=80$ MeV. To our knowledge, no previous analysis of the (d,^{6}Li) reaction has considered couplings between the ground and excited states of ^{6}Li.

Some ($\vec{d}$,^{6}Li) data, acquired utilizing polarized beams, also exist. Cross-section and VAP data have been measured for ^{24}Mg($\vec{d}$,^{6}Li)^{20}Ne and ^{40}Ca($\vec{d}$,^{6}Li)^{36}Ar at $E_d=45.5$ MeV [9] and for ^{12}C($\vec{d}$,^{6}Li)^{8}Be and ^{16}O($\vec{d}$,^{6}Li)^{12}C at $E_d=51.7$ MeV [10,11]. Data for the ^{24}Mg($\vec{d}$,^{6}Li)^{20}Ne(g.s.) and ^{40}Ca($\vec{d}$,^{6}Li)^{36}Ar(g.s.) reactions were fairly well reproduced by one-step, zero-range, DWBA calculations. One-step, finite-range, DWBA calculations provided excellent reproductions of the ^{12}C($\vec{d}$,^{6}Li)^{8}Be(g.s.) and ^{16}O($\vec{d}$,^{6}Li)^{12}C(g.s.) data. Hence, one-step analyses of ($\vec{d}$,^{6}Li) data at $E_d\approx 45$–50 MeV have shown no evidence of multistep processes in (d,^{6}Li)

reactions forming the ground states of residual nuclei.

At lower energies, Tagishi *et al.* [12] have measured the cross section, VAP, and all three TAP for ^{16}O($\vec{d}$,^{6}Li)^{12}C at E_d=22 MeV and for ^{12}C($\vec{d}$,^{6}Li)^{8}Be at E_d=18 and 22 MeV. Some of the cross-section and VAP angular distributions were fairly well reproduced by one-step, finite-range, DWBA calculations. In general, the calculated TAP compared very poorly with the data, even when a ^{6}Li D-wave admixture was included in the calculations. These analyses suggest that mechanisms other than a direct, one-step transfer of an α particle make substantial contributions in these reactions.

In Sec. II, experimental procedures for acquiring the ^{64}Zn($\vec{d}$,^{6}Li)^{60}Ni data are discussed. Section III summarizes one-step DWBA results for the ^{64}Zn(d,^{6}Li)^{60}Ni reaction and discusses the motivation for including unbound ^{6}Li continuum states in a CCBA analysis. A finite-range, CCBA treatment of the ^{64}Zn(d,^{6}Li)^{60}Ni reaction is presented in Sec. IV, and in Sec. V we discuss the results of these CCBA calculations.

II. APPARATUS AND MEASUREMENTS

A. Target selection

The target ^{64}Zn was chosen because it was the heaviest target nucleus for which sufficient yields could be obtained with E_d=16.4 MeV, the maximum deuteron bombarding energy then available at Triangle Universities Nuclear Laboratory (TUNL). Energy excitation functions of $d\sigma/d\Omega$ for (d,^{6}Li) near E_d=16 MeV on the lighter nuclei ^{36}Ar and ^{40}Ca showed fluctuations, indicating the presence of significant compound-nucleus effects. Since compound-nucleus contributions generally decrease rapidly with increasing target mass, excitation functions of $d\sigma/d\Omega$ for ^{64}Zn(d,^{6}Li)^{60}Ni were measured; no fluctuations were seen.

B. Experimental procedures

A 16.4-MeV vector- and tensor-polarized deuteron beam of typical intensity 120 nA was produced using the TUNL Lamb-shift polarized-ion source [13] and tandem Van de Graaff accelerator [14]. The beam was momentum analyzed and focussed onto a ^{64}Zn target centered in a 62-cm-diameter scattering chamber. Outgoing ^{6}Li nuclei were detected using six E-ΔE solid-state detector telescopes placed to the right-hand side of the beam in 10° intervals. Data at the odd scattering angles, θ_{lab}=25°–75°, and the even scattering angles, θ_{lab}=30°–80°, were acquired during different runs, each lasting about six days. For the two runs, the targets were composed, respectively, of 292 and 472 μg/cm^2 of 99.69% isotopically pure ^{64}Zn backed by thin (<4 μg/cm^2) layers of carbon and either aluminum or copper.

Because the ^{64}Zn(d,^{6}Li)^{60}Ni cross section is much lower than that of many other reactions emitting particles of comparable energies, background reduction measures were essential. The presence in the target of elements other than Zn (e.g., C, Al, and Cu) was minimized. At most angles, a fast coincidence requirement (10–50 ns) between signals in the E and ΔE detectors was employed. Pile-up events were rejected using the circuitry of Ortec 572 spectroscopic amplifiers. Steps were also taken to remove cross talk between detectors sharing the same ADC's. These procedures resulted in clean spectra, as seen in Fig. 1. This energy spectrum shows events at θ_{lab}=45° that were within a 2D window placed around the ^{6}Li band in the 2D, E-ΔE energy spectrum and that survived the pile-up-rejection and fast-coincidence requirements. The two peaks correspond to ^{6}Li particles recoiling from the ground and first-excited states of ^{60}Ni. Very little background is present. Bowsher [15] provides details on the background-reduction techniques.

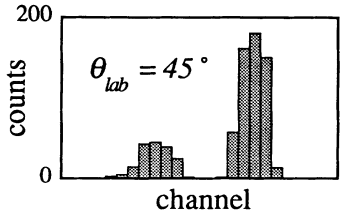

FIG. 1. Energy spectrum at θ_{lab}=45°. The larger and smaller peaks correspond to ^{64}Zn($\vec{d}$,^{6}Li) forming the ground and first-excited states of ^{60}Ni, respectively.

Cross sections and analyzing powers were obtained by measuring ($\vec{d}$,^{6}Li) count rates for each of the eight possible combinations of beam spin direction, either "up" or "down," beam hyperfine state, either "1" or "2" [16], and scattering chamber orientation, either "horizontal" or "vertical." Polarizations for the two hyperfine states were monitored continuously by a ^{3}He($\vec{d}$,p)^{4}He polarimeter placed just downstream from the scattering chamber; these polarizations were typically $P_Z^{(1)}=P_{ZZ}^{(1)}=0.60$ and $P_Z^{(2)}\approx 0, P_{ZZ}^{(2)}=-1.17$. The spin state was switched every 70 s, and the spin direction was flipped about once an hour. Bowsher [15] and Tonsfeldt [17] discuss these procedures in detail.

C. Analysis of the data

The measured cross sections and analyzing powers for the ^{64}Zn(d,^{6}Li)^{60}Ni reaction forming the ground state of ^{60}Ni are shown in Fig. 2. Data of similar quality are also available for ^{64}Zn(d,^{6}Li) forming the $I^\pi=2^+$, first excited state of ^{60}Ni [15]. The analyzing powers A_y and A_{yy} are absent at θ_{lab}=65° because of a malfunctioning detector during the chamber-horizontal portion of the experiment. The error bars represent statistical uncertainties as well as uncertainties in the polarimeter calibration. For the reaction forming the ^{60}Ni ground state these errors are typically ± 0.06 in A_y and ± 0.08 in A_{yy} and A_{xx}. For the ^{64}Zn($\vec{d}$,^{6}Li)^{60}Ni(2^+) data, typical errors are ± 0.10 in A_y and ± 0.14 in A_{yy} and A_{xx}.

For analyzing power measurements, many possible errors resulting from misalignments of the beam, misalignments of the spin symmetry axis, and inaccuracies in the current integration are reduced by placing detectors symmetrically to the left and right of the beam [18]. Symmetrically configured detectors were not employed

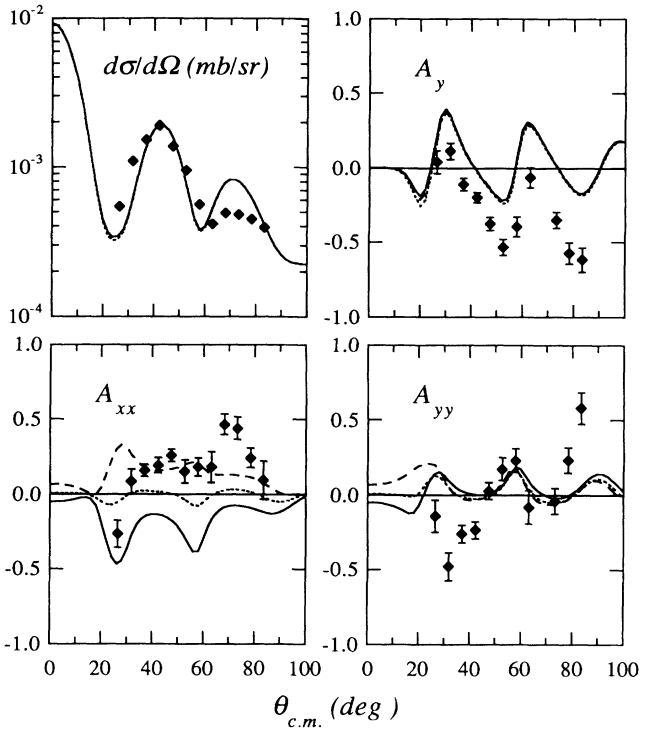

FIG. 2. Measured cross sections and analyzing powers for ^{64}Zn(d,^{6}Li)^{60}Ni(g.s.) at $E_{lab}=16.4$ MeV and finite-range, DWBA calculations of these observables. The dotted, solid, and dashed curves are generated assuming D_2 values of 0, +0.085, and −0.085 fm^2, respectively.

for the present ^{64}Zn($\vec{d}$,^{6}Li)^{60}Ni experiment because a significantly higher count rate was attainable with detectors placed to one side of the beam only. However, between the two ^{64}Zn($\vec{d}$,^{6}Li)^{60}Ni experimental runs, the ^{64}Zn($\vec{d}$,d)^{64}Zn elastic-scattering data were acquired with symmetrically placed detectors and a beam collimation system similar to that employed in the ($\vec{d}$,^{6}Li) experiments. To within statistical errors, identical results were obtained when the ($\vec{d}$,d) data were analyzed using either right-side detectors only or both left- and right-side detectors, suggesting that significant misalignments or current integration problems were not present in the experimental apparatus. The consistency, seen in Fig. 2, of the even angle (30°–80°) ($\vec{d}$,^{6}Li) data, which were acquired before the ($\vec{d}$,d) data, and the odd angle (25°–75°) ($\vec{d}$,^{6}Li) data, which were acquired after the ($\vec{d}$,d) data, also suggests that systematic errors were small compared to statistical uncertainties.

III. DWBA ANALYSIS; MOTIVATION FOR THE CCBA ANALYSIS

Shown in Fig. 2 along with the data are the results of one-step, finite-range, DWBA calculations of cross sections and analyzing powers for ^{64}Zn($\vec{d}$,^{6}Li)^{60}Ni(g.s.), performed using the code PTOLEMY [19]. The overall magnitudes of the calculated (d,^{6}Li) cross sections shown here and in other figures are adjusted to correspond roughly with that of the data. (Many considerations affect the calculated overall normalization, so that at this time we do not consider it a useful quantity for evaluating the reaction mechanisms proposed here, and we do not report the renormalizations associated with specific calculations. Typically, matching the measured cross section requires a factor of 2 increase in the calculated cross section, when spectroscopic factors of unity are assumed for all target and projectile bound states.) The deuteron and ^{6}Li distorting potentials used in these calculations are of the form

$$\begin{aligned} U(r)=&V_C(r)-V_0 f(r,r_0,a_0) \\ &-iW_S f(r,r_{WS},a_{WS})+4ia_{WD}W_D\frac{d}{dr}f(r,r_{WD},a_{WD}) \\ &+2\left[V_{SO}\frac{1}{r}\frac{d}{dr}f(r,r_{SO},a_{SO})\right. \\ &\left.+iW_{SO}\frac{1}{r}\frac{d}{dr}f(r,r_{WSO},a_{WSO})\right]\mathbf{L}\cdot\mathbf{S}\ , \end{aligned} \tag{1}$$

where the radial form factor $f(r,r_X,a_X)$ is

$$f(r,r_X,a_X)=\frac{1}{1+\exp\left[(r-r_X A^{1/3})/a_X\right]}\ . \tag{2}$$

In Eq. (1), the Coulomb interaction is $V_C(r)$, the next three terms are real volume, imaginary volume, and imaginary surface central potentials, and the last term is a complex spin-orbit potential, with **L** and **S** the orbital and spin angular momenta of the projectile. The mass number of the target nucleus is A. The globally determined parameters of Daehnick *et al.* [20] and Cook [21] are used for d-^{64}Zn and ^{6}Li-^{60}Ni elastic scattering, respectively, and are listed in Table I.

Regarding bound states, the d-α relative orbital angular momentum in the ^{6}Li ground state is predominantly $l=0$, though a small $l=2$ admixture is predicted [22,23]. Both the $l=0$ radial wave function, $u_{l l}=u_{10}$(g.s.,r), and the $l=2$ radial wave function, u_{12}(g.s.,r), are generated using the Woods-Saxon geometry of Kubo and Hirata [24], assuming one node, not counting that at the origin, in u_{10}(g.s.,r) [25,26] and zero nodes in u_{12}(g.s.,r), and adjusting the Woods-Saxon well depth to reproduce the $d+\alpha$ separation energy of ^{6}Li. A wave function φ(Zn;r_α) for the ^{60}Ni+α component of the ^{64}Zn ground state is likewise generated using the Woods-Saxon geometry of Cook [2] and assuming six nodes, which is consistent with a harmonic-oscillator shell model. Bound-state parameters are listed in Table II.

A measure of the $l=2$ admixture in the ^{6}Li ground state is provided by the parameter D_2 (Ref. [22])

$$D_2\equiv-\frac{1}{15}\frac{\int_0^\infty dr\, r^4 u_{12}(\text{g.s.},r)}{\int_0^\infty dr\, r^2 u_{10}(\text{g.s.},r)}\ . \tag{3}$$

The value $D_2=+0.085$ fm^2 was predicted by Lehman and Parke [22] on the basis of three-body ($n+p+\alpha$) calculations for ^{6}Li. On the other hand, reproducing the

TABLE I. Optical model parameters for describing ^{64}Zn(d,d)^{64}Zn and ^{60}Ni(^{6}Li,^{6}Li)^{60}Ni scattering. The parameters are defined by Eq. (1).

Interaction Lab energy	V_0 (MeV) r_0 (fm) a_0 (fm)	W_D (MeV) r_{WD} (fm) a_{WD} (fm)	W_S (MeV) r_{WS} (fm) a_{WS} (fm)	V_{SO} (MeV) r_{SO} (fm) a_{SO} (fm)	W_{SO} (MeV) r_{WSO} (fm) a_{WSO} (fm)	Source
^{64}Zn(d,d) 16.4 MeV	90.8 1.17 0.738	12.64 1.325 0.810	0	6.85 1.07 0.66	0	Daehnick *et al.*, Set L Ref. [20]
^{64}Zn(d,d) 16.4 MeV	92.8 1.17 0.769	14.46 1.325 0.792	0	8.09 1.07 0.558	2.94 1.07 0.434	Present work
^{60}Ni(^{6}Li,^{6}Li) 14.8 MeV	109.2 1.326 0.811	0	41.2 1.534 0.884	0	0	Cook Ref. [21]

^{6}Li quadrupole moment from a simple $d+\alpha$ cluster model of ^{6}Li requires a D_2 value of approximately equal magnitude but of opposite sign [23]. The dotted, solid, and dashed curves of Fig. 2 correspond to D_2 values of 0, $+0.085$, and -0.085 fm^2, respectively. These curves suggest that ($\vec{d}$,^{6}Li) A_{xx} data may be useful for measuring D_2. The DWBA calculations also indicate that the TAP A_{xz} (not shown) is sensitive to D_2. However, as discussed below, coupling to excited states of ^{6}Li appears to be important in the (d,^{6}Li) reaction, and this coupling strongly influences A_{xx} and A_{xz}. Since understanding these coupling effects is prerequisite to using ($\vec{d}$,^{6}Li) data to determine D_2, since cross section and VAP data are more useful than TAP data for studying these coupling mechanisms, and since A_{xz} measurements would have been time consuming and difficult, we chose not to measure A_{xz}.

The DWBA calculations agree fairly well with the cross-section data, but for A_y, the calculated values oscillate symmetrically about zero, whereas the data are predominantly negative. Variations of the deuteron and ^{6}Li optical potentials consistent with the deuteron and ^{6}Li elastic-scattering data were unable to reproduce the predominantly negative character of the VAP data. The DWBA results also disagree with the A_{xx} and A_{yy} TAP data, though these disagreements are less disturbing than those involving A_y, since TAP may be substantially influenced by D_2 and by optical model tensor interactions.

To account for the measured VAP, we consider coupling to excited states of ^{6}Li. Only the ground state of ^{6}Li is bound. The CCBA analysis presented in Secs. IV and V allows for α transfers forming the ground as well as unbound, continuum states of ^{6}Li. Since d and α have isospin 0, ^{6}Li states with a d-α structure must be primarily isospin 0. Below an excitation energy of 15 MeV, only three isospin-0 resonances have been identified. These have spins and parities of $I^\pi=3^+$, 2^+, and 1^+ and are predominantly $l=2$ [27]. The CCBA calculations include the ^{6}Li ground state and these three $l=2$ states. They also include four other unbound states representing the $l=0$, $I^\pi=1^+$ and the $l=1$, $I^\pi=2^-$, 1^-, and 0^- nonresonant d-α continuum states.

Two considerations motivate the inclusion of ^{6}Li continuum states. First, ^{6}Li elastic scattering is strongly influenced by projectile excitation. For example, studies of cross-section data for ^{6}Li elastic scattering at incident energies ranging from 12 to 170 MeV and on targets with mass numbers between 12 and 208 have shown that the excitation and breakup of ^{6}Li reduce the effective, single-channel, real, ^{6}Li-target, central interaction in the surface region by a factor of about 0.6 [28–30]. Also, projectile excitation has been identified as the dominant source of nonzero VAP in ^{6}Li elastic scattering on ^{58}Ni at $E_{\text{c.m.}}=12.7$, 18.1, and 20.7 MeV [31–33]. Therefore, one might also expect substantial contributions to (d,^{6}Li) reactions from α transfers through excited states of ^{6}Li.

Second, DWBA calculations, performed using the code PTOLEMY, indicate that one-step α transfers forming $l=2$, $I^\pi=3^+$, 2^+, and 1^+ states of ^{6}Li are highly spin dependent. The dotted curves of Fig. 3 show DWBA calculations of A_y, A_{yy}, A_{xx}, and A_{xz} for α transfers form-

TABLE II. Optical model parameters specifying the geometry of the bound-state potentials.

Bound state	r_0 (fm)	a_0 (fm)	Source
^{6}Li$\rightarrow d+\alpha$	1.2	0.65	Kubo and Hirata, Ref. [24][a]
^{64}Zn$\rightarrow^{60}$Ni$+\alpha$	1.2	0.65	Cook, Ref. [2][a]
^{64}Zn$\rightarrow^{60}$Ni$+\alpha$	1.42	1.19	Budzanowski, Ref. [34][b]

[a]Parameters are defined by Eq. (1).
[b]Parameters are defined by Eq. (18).

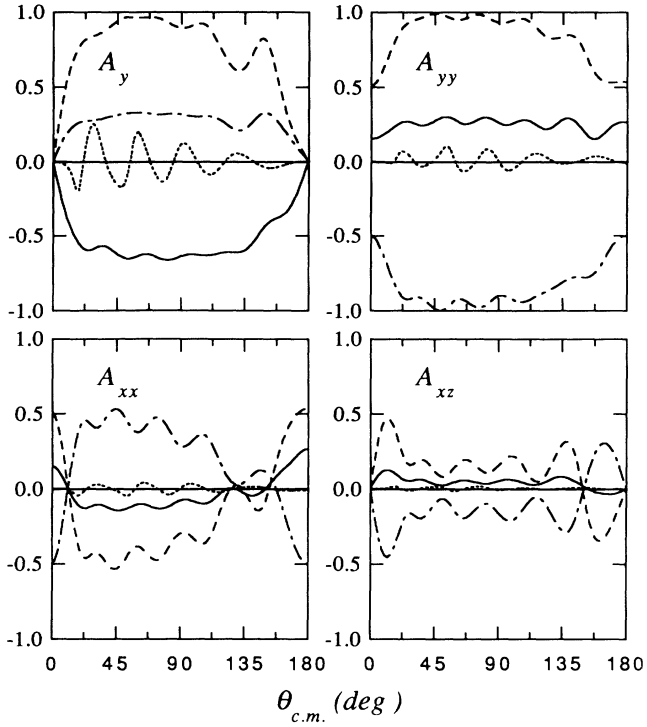

FIG. 3. Calculated analyzing powers for one-step, ^{64}Zn$(d,^6$Li$)^{60}$Ni forming various ^{6}Li configurations. The calculation corresponding to the dotted curves assumes a pure $l=0$, $I^\pi=1^+$ ^{6}Li ground state. The solid, dash-dotted, and dashed curves are obtained by artificially assigning to the ^{6}Li ground state a $d+\alpha$ orbital angular momentum of $l=2$ and, respectively, spins and parities of $I^\pi=3^+$, 2^+, and 1^+.

ing the ($l=0$, $I^\pi=1^+$) ^{6}Li ground state. In Sec. IV, we present a proper treatment of the ^{6}Li continuum; for now, we obtain a rough prediction of the spin dependence of α transfers forming $l=2$ ^{6}Li resonant states by artificially assigning this orbital angular momentum to the ^{6}Li ground state. Hence, the solid, dash-dotted, and dashed curves are DWBA results for α transfers forming pure $l=2$, $I^\pi=3^+$, 2^+, and 1^+ ^{6}Li configurations, respectively. For the $\Delta l=0$ transfer, the analyzing powers are small and oscillate symmetrically about zero. In contrast, the analyzing powers for $\Delta l=2$ transfers reveal strong preferences for certain spin orientations. We note in particular that the VAP for the transfer forming the 3^+ configuration is, like the measured ^{64}Zn$(\vec{d},^6$Li$)^{60}$Ni(g.s.) data, quite negative. These spin dependences may be understood in terms of simple momentum matching considerations [15]. The results shown in Fig. 3 suggest that it is necessary to incorporate ^{6}Li excited-state configurations in order to clarify their influence on the spin dependence of the ground-state transfer reaction.

IV. CCBA ANALYSIS OF THE ^{64}Zn$(d,^6$Li$)^{60}$Ni REACTION

A. The transition amplitude

The amplitude for an incident deuteron, with a spin projection σ, initiating the ^{64}Zn$(d,^6$Li$)^{60}$Ni reaction producing ^{6}Li with spin projection Σ can be written, in the coupled-channels Born approximation (CCBA), as

$$T_{\Sigma\sigma}^{\rm CCBA}=\langle\Psi_{\rm Li\Sigma}^{(-)}(\mathbf{R},\mathbf{r})|V_{d\alpha}(\mathbf{r}) +[V_{d\rm Ni}(\mathbf{r}_d)-U_d(\mathbf{R}_d)]|\varphi(\rm Zn;\mathbf{r}_\alpha)\chi_{d\sigma}^{(+)}(\mathbf{R}_d)\rangle \quad (4)$$

where $\mathbf{r}$ and $\mathbf{r}_\alpha$ are the d-α and α-^{60}Ni relative coordinates, respectively, and $\mathbf{R}_d$ and $\mathbf{R}$ are the deuteron- and ^{6}Li-nucleus separations in the initial and final states. Figure 4 presents the various coordinates.

In the following, Eq. (4) is estimated consistently within the $d+\alpha+$residual nucleus, three-body model, and thus the microscopic $d+\alpha$ and $d+^{60}$Ni transition interactions, $V_{d\alpha}$ and $V_{d\rm Ni}$, appearing in Eq. (4) are understood as two-body interactions. In Eq. (4), U_d is the d-^{64}Zn interaction that generates $\chi_{d\sigma}^{(+)}$, which describes the center-of-mass motion of the incident deuteron, and $\psi_{\rm Li\Sigma}^{(-)}$ is the coupled-channels wave function for the ^{6}Li-^{60}Ni system. Which channels are included explicitly in this coupled-channels treatment of the final state is discussed fully in Sec. IV B. However, as discussed in Secs. I and III, one of our main aims in this work is to examine the role in the transfer process of the low-lying states of the $d+\alpha$ system, particularly the $l=2$ resonant states. Inclusion of the $l=2$ states precludes the use of zero-range approximations in the transfer-reaction element of the calculations. Finite-range CCBA calculations are undertaken using the computer code FRESCO [1].

The potential $U_d(\mathbf{R}_d)$ is obtained by adjusting slightly the globally determined, set-L optical model interactions of Daehnick, Childs, and Vrcelj [20] to fit the present deuteron elastic-scattering cross-section and VAP data. Parameters specifying this interaction are given in Table I. The ^{60}Ni$+\alpha$ bound-state wave function $\varphi(\rm Zn;\mathbf{r}_\alpha)$ is calculated from the real part of the α-nucleus potential parametrization of Budzanowski *et al.* [34] (Table II). The potential depth is adjusted so that the wave function, with six nodes, reproduces the empirical ^{60}Ni$+\alpha$ separation energy (3.956 MeV) in the ^{64}Zn ground state. The so-called remnant term in the transition interaction, $V_{d\rm Ni}(\mathbf{r}_d)-U_d(\mathbf{R}_d)$, is neglected in the following. Its importance was estimated by replacing the d-^{60}Ni interaction $V_{d\rm Ni}(\mathbf{r}_d)$ by the optical potential $U_d(\mathbf{r}_d)$, evaluated at the correct d-^{60}Ni separation $\mathbf{r}_d$; the effects were small in comparison with other uncertainties in the calculation.

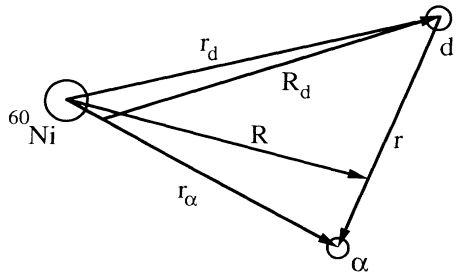

FIG. 4. Coordinates employed in the finite-range, CCBA analysis of ^{64}Zn$(d,^6$Li$)^{60}$Ni. The separation of d and the ^{64}Zn center of mass is R_d, and R is the separation of ^{6}Li and the ^{60}Ni center of mass.

The choice and treatment of those coupled channels included in the final state, and of the corresponding $d+\alpha$ interactions $V_{d\alpha}$, are the subject of Sec. IV B.

B. Coupled-channels treatment of the ^{6}Li-^{60}Ni system

The ^{6}Li-^{60}Ni system is considered within the coupled-channels formalism, in which we allow the ground state of the outgoing ^{6}Li projectile to couple to a chosen set of intrinsic states of $d+\alpha$ relative motion. Within the $d+\alpha$ cluster model, such states of the $d+\alpha$ (^{6}Li) system with total spin I, projection Σ, and relative orbital angular momentum l can be written

$$\varphi_l^{I\Sigma}(\mathbf{r})=\sum_{\lambda\sigma'}(l\lambda 1\sigma'|I\Sigma)u_{Il}(r)Y_{l\lambda}(\hat{r})\chi_1^{\sigma'} , \tag{5}$$

where $\chi_1^{\sigma'}$ is the deuteron spin wave function. Since the DWBA calculations of Sec. III show that the D-state component of the ^{6}Li ground state has only very small effects on the transfer reaction cross section and VAP, the CCBA calculations do not include this D-state component explicitly. Thus, the ground state wave function is also defined by Eq. (5) and is denoted $\varphi_0^{1\Sigma}$(g.s.,$\mathbf{r}$), with radial wave function u_{10}(g.s.,r). For the unbound states of the $d+\alpha$ (^{6}Li) system, the radial functions $u_{Il}(r)$ are normalized such that asymptotically

$$u_{Il}(r)\rightarrow\sqrt{2/\pi}\sin[kr-\eta\ln(2kr)-\tfrac{1}{2}l\pi+\sigma_l(\eta)+\delta_{Il}] , \tag{6}$$

where $\sigma_l(\eta)$ is the Coulomb phase shift, η the Coulomb parameter, and δ_{Il} the nuclear phase shift. To make explicit the dependence of these intrinsic states on the $d+\alpha$ relative energy, in the following we denote the total wave function for these states by $\varphi_l^{I\Sigma}(k,\mathbf{r})$.

Our treatment of the ^{6}Li-residual nucleus system follows closely that of Sakuragi and the Kyushu University group [28,29]. In terms of the complete set of states of $d+\alpha$ relative motion introduced above, the wave function $\psi_{\mathrm{Li}\Sigma}^{(+)}(\mathbf{R},\mathbf{r})$—we use outgoing-wave boundary conditions for clarity—can be expanded as

$$\psi_{\mathrm{Li}\Sigma}^{(+)}(\mathbf{R},\mathbf{r})=\sum_{\Sigma'}\chi_{\Sigma'\Sigma}(P_0,\mathbf{R})\varphi_0^{1\Sigma'}(\mathrm{g.s.},\mathbf{r}) + \sum_{Il\Sigma'}\int dk\,\chi_{\Sigma'\Sigma}^{Il}(P_k,\mathbf{R})\varphi_l^{I\Sigma'}(k,\mathbf{r}) , \tag{7}$$

where the $\chi_{\Sigma'\Sigma}$ describe the motion of the center of mass of the $d+\alpha$ system for each relative motion state, with P_k the associated asymptotic center-of-mass momentum of that state. In keeping with the usual coupled-discretized continuum-channels (CDCC) treatment of the $d+\alpha$ continuum, the integral in k is discretized into a finite set of momentum bins, the upper and lower limits on a particular bin i being $k_i^>$ and $k_i^<$, respectively. Omitting the spin projection quantum numbers for simplicity, we thus write

$$\psi_{\mathrm{Li}}^{(+)}(\mathbf{R},\mathbf{r})=\chi(P_0,\mathbf{R})\varphi_0^1(\mathrm{g.s.},\mathbf{r}) + \sum_{Ili}\int_{k_i^<}^{k_i^>}dk\,\chi^{Il}(P_k,\mathbf{R})\varphi_l^I(k,\mathbf{r}) . \tag{8}$$

Following Sakuragi, the energy dependence of the center-of-mass wave functions $\chi^{Il}(P_k,\mathbf{R})$ can be accurately factored out. Thus one writes

$$\chi^{Il}(P_k,\mathbf{R})\approx f_{Ili}(k)\chi^{Il}(P^i,\mathbf{R}) , \tag{9}$$

where P^i is calculated at the mean energy in bin i. Over moderate energy intervals and in nonresonant regions the $\chi^{Il}(P_k,\mathbf{R})$ are essentially energy independent, suggesting that $f_{Ili}(k)=1$. In the region of a resonance we use $f_{Ili}(k)=\sin\delta_{Il}(k)$, with $\delta_{Il}(k)$ the nuclear phase shift. Other authors [28,29] have used slightly different prescriptions for the $f_{Ili}(k)$, however our results are insensitive to such details.

Within the above approximations, one can translate the $d+\alpha$ continuum problem into a finite discrete-states coupled-channels problem, written

$$\psi_{\mathrm{Li}}^{(+)}(\mathbf{R},\mathbf{r})=\chi(P_0,\mathbf{R})\varphi_0^1(\mathrm{g.s.},\mathbf{r})+\sum_{Ili}X_i^{Il}(P^i,\mathbf{R})\Phi_{li}^I(\mathbf{r}) , \tag{10}$$

by defining the center-of-mass functions

$$X_i^{Il}(P^i,\mathbf{R})=\sqrt{N_{Ili}}\chi^{Il}(P^i,\mathbf{R}) , \tag{11}$$

and intrinsic $d+\alpha$ relative motion states

$$\Phi_{li}^I(\mathbf{r})=\frac{1}{\sqrt{N_{Ili}}}\int_{k_i^<}^{k_i^>}dk\,\varphi_l^I(k,\mathbf{r})f_{Ili}(k) , \tag{12}$$

where the normalization factors N_{Ili} are

$$N_{Ili}=\int_{k_i^<}^{k_i^>}dk\,[f_{Ili}(k)]^2 . \tag{13}$$

As constructed, these intrinsic bin states $\Phi_{li}^I(\mathbf{r})$ and the ^{6}Li ground state form an orthonormal square-integrable set of states

$$\begin{aligned}&\langle\Phi_{li}^I|\Phi_{l'i'}^{I'}\rangle=\delta_{II'}\delta_{ll'}\delta_{ii'} ,\\ &\langle\Phi_{li}^I|\varphi_0^1(\mathrm{g.s.})\rangle=0 ,\end{aligned} \tag{14}$$

with the result that the coupled-channels calculation can be carried out using conventional techniques.

In line with previous applications of the CDCC method to ^{6}Li elastic scattering, we include $l=0$, 1, and 2 relative motion states of the $d+\alpha$ continuum. The nonresonant, low-energy $l=0$ and $l=1$ ($I^\pi=2^-$, 1^-, and 0^-) states are treated approximately by placing, for each angular momentum coupling (l,I^π), one bin on the interval 0.05 fm$^{-1}\le k\le$0.55 fm^{-1}, corresponding to $d+\alpha$ relative energies 0.039 MeV$\le\varepsilon\le$4.722 MeV and a mean energy of 3.85 MeV above the ^{6}Li ground state. For the $l=2$ states, bins of widths 0.03, 2.0, and 3.0 MeV are placed on the $I^\pi=3^+$, 2^+, and 1^+ states, respectively, whose empirical widths are 0.020±0.003, 1.32±0.04, and 1.9±0.1 MeV [27,35], so as to include all significant coupling strength to the resonant states. The mean energies of these resonant state bins are 2.185, 4.36, and 5.3 MeV above the energy of the ^{6}Li ground state [27,35].

The interaction $V_{d\alpha}$ used in generating the $d+\alpha$ relative motion configurations is assumed to be of the form

$$V_{d\alpha}(\mathbf{r})=V_C(\mathbf{r})-\frac{V}{1+\exp[(r-R_0)/a]}\ , \tag{15}$$

with V_C the Coulomb interaction of a uniform charge distribution of radius 1.9 fm and R_0 and a taken from the work of Kubo and Hirata [24]. The depth V, which is state dependent, is adjusted to 85.02 MeV for the narrow $I^\pi=3^+$ state, so as to reproduce the resonance energy, and to 77.05 MeV for the ^{6}Li ground state, to reproduce its $d+\alpha$ separation energy. Potential depths for the remaining continuum states are adjusted to produce, over the range of $d+\alpha$ energies considered here, scattering phase shifts in accord with those determined by Schmelzbach *et al.* [36].

Having defined the intrinsic states φ_0^l(g.s.) and Φ_{li}^I of the $d+\alpha$ system, the channel coupling and diagonal channel interactions entering the coupled equations for the $X_i^{Il}(P^i,\mathbf{R})$ and $\chi(P_0,\mathbf{R})$ can be calculated from the underlying deuteron-^{60}Ni and α-^{60}Ni interactions. That is, we evaluate the continuum-continuum coupling potentials as

$$U_{lil'i'}^{II'}(\mathbf{R})=\langle\Phi_{li}^I|U^{\text{eff}}|\Phi_{l'i'}^{I'}\rangle\ , \tag{16}$$

and similarly for the ground-state–to–ground-state and ground-state–to–bin-state terms, where

$$U^{\text{eff}}(\mathbf{R},\mathbf{r})=N_R[V_{d\text{Ni}}+V_{\alpha\text{Ni}}]+N_I[W_{d\text{Ni}}+W_{\alpha\text{Ni}}]\ , \tag{17}$$

with V and W the real and imaginary parts of the interactions, assumed to be phenomenological optical potentials. Cluster model calculations for the $d+\alpha+$Ni system at energies near the Coulomb barrier have shown that detailed agreement with cross-section data is not obtained unless the folded potentials are renormalized [31,32]. For generality we thus include the renormalization factors N_R and N_I for the real and imaginary parts; however, unless stated otherwise, these are set to unity.

The deuteron-^{60}Ni interaction is taken from the global parametrization (set L) of Daehnick, Childs, and Vrcelj [20]. We note, however, that the deuteron energy required, $E_d=\frac{1}{3}E_{\text{Li}}\approx 5$ MeV, lies outside the range of data incorporated in that global fit, namely, 11.8 MeV $\leq E_d\leq 90$ MeV. A similar problem is encountered with the α-^{60}Ni interaction, where we require the potential at $E_\alpha=\frac{2}{3}E_{\text{Li}}\approx 10$ MeV. We obtain this potential from the Woods-Saxon squared, global parametrization of Budzanowski *et al.* [34], which describes ^{58,60}Ni α-scattering data over an energy range 26.5 MeV $\leq E_\alpha\leq$ 139 MeV. Thus we assume

$$U_{\alpha\text{Ni}}(r)=V_C(r)-V_0f^2(r,r_0,a_0)-iW_Sf^2(r,r_{WS},a_{WS}) \tag{18}$$

with f the conventional Woods-Saxon form factor, defined by Eq. (2). The Coulomb interaction V_C is taken to be that of a uniformly charged sphere of radius $1.34A^{1/3}$. Budzanowski *et al.* avoided discrete ambiguities in their α potentials by requiring a real potential volume integral of near 300 MeV fm^3, the value determined by $E_\alpha=139$ MeV nuclear rainbow scattering [37,38]. The deuteron and α-particle potential parameters are collected in Table III.

C. Calculations for ^{6}Li-^{60}Ni elastic scattering

As a limited check of our description of the ^{6}Li-^{60}Ni final-state, coupled-channels predictions for the elastic-scattering observables are compared to data. As just noted, the application of the cluster-folding approach to the ^{6}Li-nucleus problem at low energies is ambiguous because of the lack of elastic-scattering data, and consequently of phenomenological optical potentials, for the constituent cluster-target systems at the required energies.

The most complete analyses of the application of the cluster model to low-energy ^{6}Li scattering are the works of Nishioka *et al.* [31] and Ohnishi *et al.* [32]. The latter authors included precisely those coupled channels that are treated here, while Nishioka *et al.* considered only the three $l=2$ resonance states. In both analyses however, the coupled-channels calculations underestimated the back-angle cross sections, and a renormalization of the folded interactions, Eq. (16), was required in order to obtain an accurate reproduction of the cross-section data. The extent to which this discrepancy is caused by omitted channels, such as Coulomb breakup, which may be strong near the Coulomb barrier, has yet to be clarified. Applications of the cluster folding model at higher energies on the other hand, such as the work of Thompson and Nagarajan at 156 MeV, provide a good reproduction of cross-section data without the need for renormalization of the calculated potentials [39].

In Fig. 5 we show the cluster model coupled-channels

TABLE III. Optical model parameters utilized for folding model calculations.

Interaction Lab energy	V_0 (MeV) r_0 (fm) a_0 (fm)	W_D (MeV) r_{WD} (fm) a_{WD} (fm)	W_S (MeV) r_{WS} (fm) a_{WS} (fm)	Source
^{60}Ni(d,d) 4.9 MeV	93.52 1.17 0.738	12.30 1.325 0.804	0	Daehnick *et al.*, Set L Ref. [20][a]
^{60}Ni(α,α) 9.8 MeV	154.9 1.42 1.19	0	28.6 1.33 0.407	Budzanowski Ref. [34][b]

[a]Parameters are defined by Eq. (1).
[b]Parameters are defined by Eq. (18).

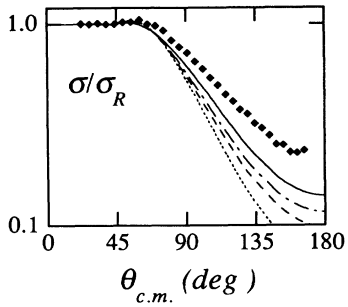

FIG. 5. Measured and predicted cross sections for ^{60}Ni(^{6}Li,^{6}Li)^{60}Ni elastic scattering at $E_{lab}=14.8$ MeV. Results are expressed as fractions of the Coulomb scattering cross sections. The dotted, dashed, dash-dotted, and solid curves correspond to calculations including the ^{6}Li ground state only, the ground and 3^+ states, the ground, 3^+, 2^+, and 1^+ ($l=2$) states, and all eight ^{6}Li states, respectively. For all four calculations, $N_R=N_I=1$.

calculations of the present work for the ^{60}Ni(^{6}Li,^{6}Li)^{60}Ni cross section at $E_{lab}=14.8$ MeV. The four curves correspond to calculations that include only the ^{6}Li ground state (dotted curve), the ground state and the $I^\pi=3^+$ resonance state (dashed curve), the ground state and the $l=2$, $I^\pi=3^+$, 2^+, and 1^+ resonance states (dash-dotted curve), and all eight $l=0$, 1, and 2 configurations (solid curve). These calculations assume $N_R=N_I=1$ for the normalization factors of Eq. (17). With the inclusion of each additional inelastic configuration the calculated cross section moves closer to the data. However, even our eight-channel calculation underestimates the measured back-angle cross sections. As stated above, this result is consistent with other analyses in the energy regime $E_{lab}\leq 23$ MeV and suggests that not all inelastic channels have been adequately described. The calculations can be made to agree precisely with the measured cross section by a suitable renormalization of the cluster folding potentials. The data however, because of their lack of angular structure and their relatively small departures from Rutherford scattering, do not allow one to distinguish between many possible choices of N_R and N_I, all of which provide equally good descriptions of these data. For example, the choices (N_R,N_I) = (0.5,0.7) and (0.7,0.4) both describe the data well.

In concluding this section, we note that if one obtains the ^{60}Ni(^{6}Li,^{6}Li)^{60}Ni cross section at 14.8 MeV not from a coupled-channels calculation, as above, but rather from a single-channel calculation that employs the phenomenological ^{6}Li optical potential parametrization of Cook [21], the resulting cross section is essentially identical to that of our eight-state coupled-channels calculation (solid curve of Fig. 5). As with the deuteron- and α-nucleus potentials, used as input to the coupled-channels calculations, the Cook potential was derived by fitting higher-energy elastic-scattering data. The nearly identical failures of both the cluster-folding model approach and the phenomenological approach to reproduce the data highlight the danger of extrapolating interactions deduced from higher-energy data to energies near the Coulomb barrier and also the need for elastic-scattering analyses of the cluster-target systems at the appropriate energies. We shall return in the next section to a discussion of the potential ambiguities inherent in our CCBA analysis of the ^{64}Zn(d,^{6}Li)^{60}Ni reaction.

V. RESULTS FOR THE ^{64}Zn(d,^{6}Li)^{60}Ni REACTION

To gain a first impression of the relative importance of transfers to the various $d+\alpha$ final-state configurations, we compare in Fig. 6 calculated DWBA cross sections for one-step α transfers forming the ^{6}Li ground state and each of the seven $l=0$, 1, and 2 continuum states. Distortion effects in the ^{6}Li-^{60}Ni partition are described using the potentials of Table I. The calculation for the transfer forming the ($l=0$) ^{6}Li ground state (dashed curve) is identical to that of Fig. 3, while calculations for the $l=2$ states (solid curves) differ from those of Fig. 3 in that here we describe the ^{6}Li continuum with the wave functions $\Phi_{li}^I(\mathbf{r})$ of Eq. (12). We observe that the cross section for producing the $I^\pi=3^+$ state is comparable in magnitude to that for the ground-state transition, but that the transfer cross sections to the remaining bin states are small. These cross-section calculations suggest that, at the ^{6}Li energy of interest here (14.8 MeV), transfer to the 3^+ resonance is important and, moreover, dominates over transfers forming the other $d+\alpha$ continuum configurations.

The effects of various α-transfer routes on observables for the ^{64}Zn(d,^{6}Li)^{60}Ni(g.s.) reaction depend not only on the strengths of these α transfers but also on the strengths and phases entering the couplings of the excited $d+\alpha$ configurations to the ^{6}Li ground state. These factors are treated consistently here within the CCBA. In Fig. 7 we present ground-state-transfer observables ob-

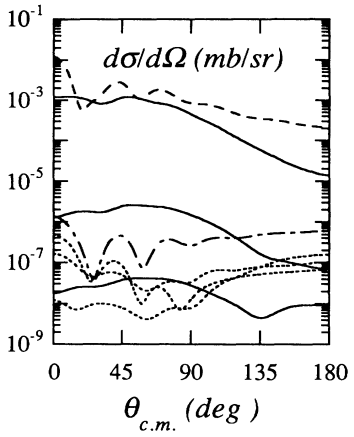

FIG. 6. Calculated cross sections for one-step, ^{64}Zn(d,^{6}Li)^{60}Ni forming the ground and the seven continuum bin states of ^{6}Li. The dashed curve indicates the differential cross section for formation of the ground state. The three solid curves represent cross sections for forming the $l=2$ resonance states, with the transfer to the 3^+ state having the highest cross section and that to the 1^+ state the lowest. The cross section for forming the $l=0$ continuum state is specified by the long-dashed-short-dashed curve, and the dotted curves are for transfers forming the $l=1$ continuum states.

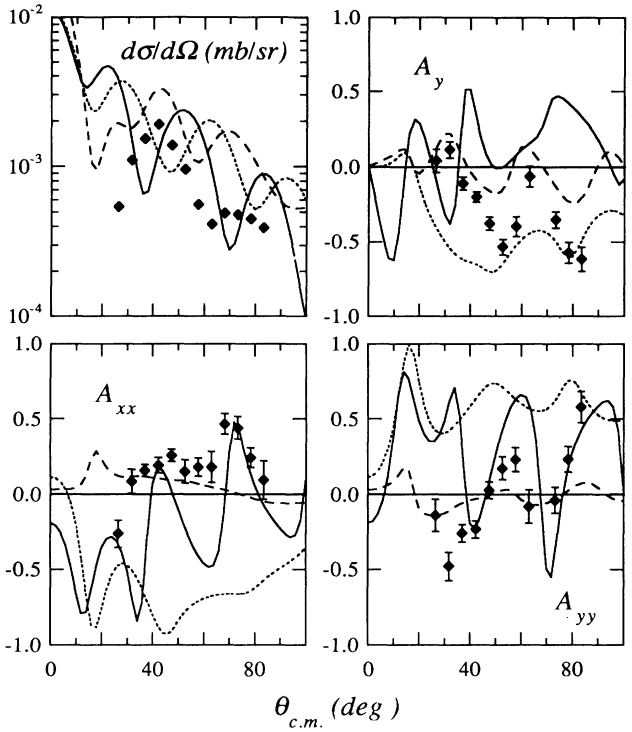

FIG. 7. The results of finite-range, CCBA ^{64}Zn(d,^{6}Li)^{60}Ni calculations involving the ^{6}Li ground and 3^+ states. The dashed, dotted, and solid curves correspond to calculations allowing for transfers forming the ground state only, the 3^+ state only, and both states, respectively, as illustrated in Fig. 8. All three calculations allow for couplings between the ground and 3^+ states.

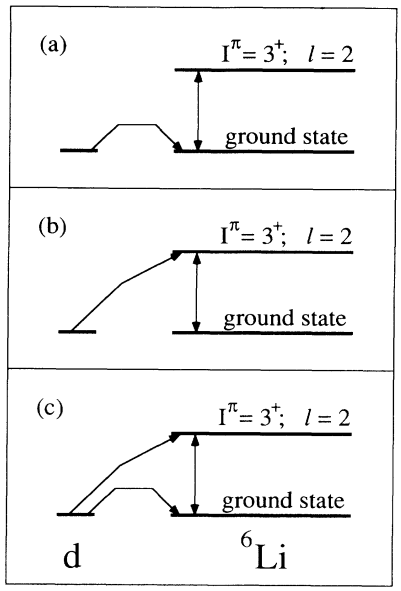

FIG. 8. Schematic diagram of the couplings considered in the calculations of Fig. 7. Parts (a), (b), and (c) indicate the couplings allowed in the calculations associated with the dashed, dotted, and solid curves of Fig. 7.

tained from finite-range, CCBA calculations that include only the ^{6}Li ground and 3^+-resonance states. The dashed, dotted, and solid curves correspond to calculations that allow for α transfers forming the ground state only, the 3^+ state only, and both states, respectively, as illustrated in Fig. 8. All three calculations include channel coupling between the ground and 3^+ states. As with all the CCBA calculations presented below, interactions within the ^{6}Li-^{60}Ni partition are generated using the folding model specified by Eq. (16). Figure 7 indicates a considerable contribution to the ground-state-transfer cross section from α transfer through the intermediate 3^+ configuration, comparable with that from direct transfer into the ground state. As we expect from the DWBA results discussed in Sec. III and shown in Fig. 3, the path through the 3^+ state (dotted curve) produces a predominantly negative A_y, while the direct transfer to the ^{6}Li ground state yields an A_y angular distribution that oscillates symmetrically about zero. The full CCBA calculation (solid curves) introduces the interference between these two paths. The calculation predicts a predominantly positive VAP, rather than the predominantly negative value required by the data. The positive A_{yy} and negative A_{xx} of the pure 3^+-state transfer (dotted curve) are also anticipated, though the magnitudes of these TAP's are significantly larger here. The calculations associated with Fig. 7 employ no rescaling of the final-state coupling interactions, i.e., $(N_R,N_I)=(1.0,1.0)$. The use of renormalized (lower) values of (N_R,N_I), such as reproduce accurately the ^{6}Li elastic-scattering data, reduce the channel coupling and consequently the effects of the 3^+ state. The major features of the solid curves in Fig. 7, such as positive VAP, remain, although they are somewhat less prominent.

Figure 9 presents the results of CCBA calculations which include transfer to and coupling among all eight ^{6}Li final states. These calculations assume the following renormalizations of the final-state interactions: (N_R,N_I) $=(1.0,1.0)$ (solid curves), (0.5,0.7) (dotted curves), and (0.7,0.4) (dashed curves). Consideration of the solid curves in Figs. 7 and 9 allows a comparison of CCBA calculations involving only the ^{6}Li ground and 3^+ states with CCBA calculations involving all eight final-state configurations. The predicted values of A_y are much more predominantly positive with the eight-state calculations. The primary source of this change in A_y is that in allowing for channel coupling among all eight ^{6}Li final-state configurations, the eight-state calculations (Fig. 9) treat distortion effects more completely than do the two-channel calculations (Fig. 7). We made several other CCBA calculations, the results of which are not shown, that allowed for coupling among all eight ^{6}Li states while restricting in various ways the final states to which direct transfer could occur. These calculations indicate that α transfers forming the other six ^{6}Li configurations have relatively small effects on A_y. That is, the strongly positive A_y values predicted by the eight-state CCBA calculations (Fig. 9) are mainly a consequence of interference between the two paths involving α transfers to the ^{6}Li ground and 3^+ states. On the other hand, the additions

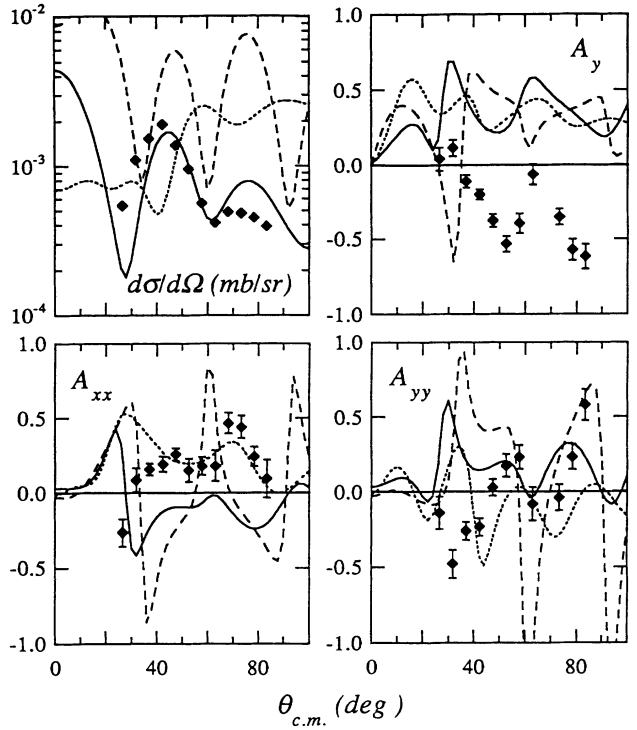

FIG. 9. The results of finite-range, eight-state, CCBA ^{64}Zn(d,^{6}Li)^{60}Ni calculations. These calculations include transfers forming and couplings between the ^{6}Li ground state and the seven ^{6}Li continuum bin states. The dotted, dashed, and solid curves correspond to the assumptions (N_R,N_I) $=(0.5,0.7),(0.7,0.4)$, and (1.0,1.0), respectively.

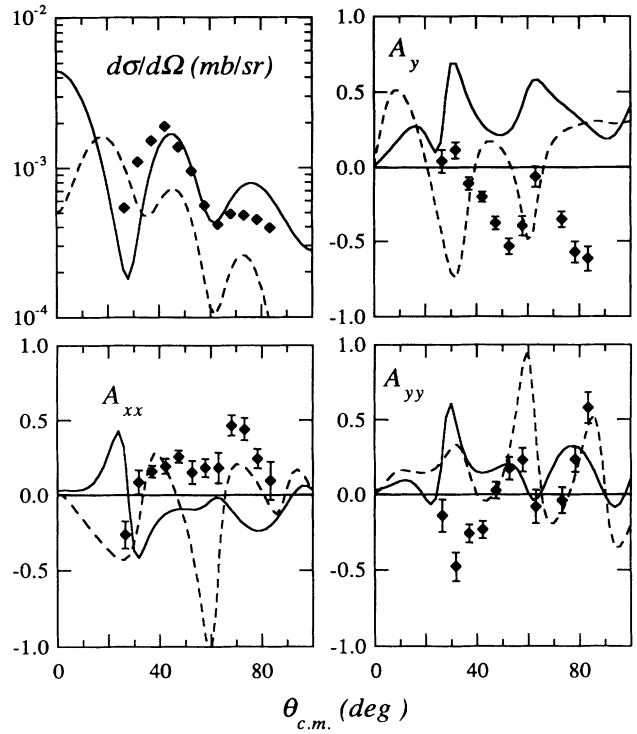

FIG. 10. The solid curves are identical to those of Fig. 9. The calculation associated with the dashed curves differs only in that the α-^{60}Ni optical potentials are taken from Trombik *et al.* [40] rather than from Budzanowski *et al.* [34].

of both α transfer to and channel coupling with the remaining six ^{6}Li configurations are important sources of the different values of $d\sigma/d\Omega$, A_{xx}, and A_{yy} shown by the solid curves of Figs. 7 and 9.

As discussed in Sec. IV, our eight-state CC calculations do not reproduce the ^{60}Ni(^{6}Li,^{6}Li)^{60}Ni data when we maintain the values $(N_R,N_I)=(1.0,1.0)$. Good fits are obtained with various renormalizations of the potentials, including (0.5,0.7) and (0.7,0.4), and one might expect that the ($\vec{d}$,^{6}Li) data could be better reproduced using these renormalized interactions. The results of such calculations are shown by the dotted and dashed curves of Fig. 9. The renormalizations destroy the agreement with the cross-section data, which are best reproduced by the calculation with $(N_R,N_I)=(1.0,1.0)$. In addition, rescaling of the interactions does not change the sign of the calculated (d,^{6}Li) VAP. It does strongly affect the TAP. Additional choices of renormalization, spanning a wide range of (N_R,N_I) values, did not reproduce the VAP data.

The sensitivity of the calculations to our final-state description is further illustrated by Fig. 10. The solid curves are identical to those of Fig. 9. The dashed curves correspond to eight-channel CCBA calculations in which the cluster-folding potentials are obtained from the α-particle optical potentials of Trombik *et al.* [40] rather than from Budzanowski *et al.* [34]. Otherwise, the calculations associated with the dashed and solid curves are identical. Trombik *et al.* assumed an interaction of the form

$$U_{\alpha\mathrm{Ni}}(r)=V_C(r)-(V+iW)f(r,r_0,a_0)\ , \tag{19}$$

the Coulomb interaction being that from a uniformly charged sphere of radius $1.65A^{1/3}$ fm. They found that ^{58,60,62,64}Ni(α,α) data at $E_{\mathrm{lab}}=18$, 21, 24.1, and 27 MeV are well reproduced by the values $V=41.4$ MeV, $W=8.4$ MeV, $r_0=1.65$ fm, and $a_0=0.52$ fm. Use of the Trombik potentials results in significantly different VAP's. The real volume integral for this interaction is 207 MeV fm^3, compared with 300 MeV fm^3 for the potentials of Budzanowski *et al.* As discussed in Sec. IV, ambiguities in the volume integral have been resolved, in favor of the interactions of Budzanowski *et al.*, by high energy (139 MeV) (α,α) scattering data and by careful extension of these volume integrals to lower energies [34,37,38]. Yet, because of the degree of extrapolation that we require, down to Coulomb barrier energies, our use of the Budzanowski *et al.* volume integrals may be suspect. Both Fig. 10 and the ^{6}Li elastic-scattering results (Fig. 5) indicate that the required cluster-target interactions are not sufficiently well determined at the energies considered here.

VI. DISCUSSION AND CONCLUSIONS

It is becoming increasingly evident that excitations of low-lying states of the projectile and target play an important part in the reaction mechanisms and spin depen-

dences of heavy-ion collisions. The $(d,{}^6\mathrm{Li})$ reaction provides a good prototype for studying the role of such inelastic excitation processes in transfer reactions involving composite projectiles. The sparseness of isospin-0 ^{6}Li excited states means that explicit inclusion of projectile excitation effects in $(d,{}^6\mathrm{Li})$ calculations is tractable. Also, the composite $(d+\alpha)$ structure of ^{6}Li is better understood than that of most heavy ions. From the experimental point of view, polarized deuteron and ^{6}Li beams are available, allowing measurements of both the $(d,{}^6\mathrm{Li})$ and the inverse $({}^6\mathrm{Li},d)$ analyzing powers. As is evident from the present work, analyzing-power data provide considerable information regarding reaction mechanisms. Finally, deuteron elastic scattering is well understood, in comparison with that of heavier ions, so that uncertainties associated with distortion effects in the deuteron channel are minimized, and as mentioned in Sec. IV C, ^{6}Li elastic scattering is also well studied.

For several reasons, an improved understanding of the $(d,{}^6\mathrm{Li})$ reaction is desirable in its own right. For instance, one-step transfer calculations (see, e.g., Fig. 2) show that reaction tensor analyzing powers are sensitive to small D-state ($l=2$) admixtures in the ^{6}Li ground state wave function. A measurement of this D-state admixture would provide an important test of the predictions of the cluster and three-body $(\alpha+n+p)$ models of ^{6}Li. A prerequisite to any possible extraction of this admixture from $(\vec{d},{}^6\mathrm{Li})$ data is, however, an understanding of the role of $l=2$ states in the $d+\alpha$ continuum, since transfers to these configurations strongly influence the TAP. Also, a better understanding of the mechanisms of $(d,{}^6\mathrm{Li})$ and other α-transfer reactions would improve the determination of α spectroscopic factors.

In this paper we have presented cross-section and vector (A_y) and tensor analyzing power (A_{yy} and A_{xx}) data for $^{64}\mathrm{Zn}(d,{}^6\mathrm{Li})$, at $E_d=16.4$ MeV, forming the ground and first-excited states of ^{60}Ni. We have shown that the predominantly negative VAP data are not reproduced by finite-range DWBA calculations, and that transfer through the $l=2$, $I^\pi=3^+$ final state of the $d+\alpha$ system could account for this spin selectivity. The effects of projectile excitation channels on ^{6}Li elastic scattering have been extensively studied within the $d+\alpha$ cluster model through coupled-channels treatments. In the present work also, our coupled-channels calculations accurately reproduce VAP data for $^{58}\mathrm{Ni}({}^6\mathrm{Li},{}^6\mathrm{Li})^{58}\mathrm{Ni}$ elastic scattering at $E_{\mathrm{c.m.}}=18.1$ and 20.7 MeV, and our calculated cross sections and VAP's agree with the cluster model, coupled-channels results obtained by Nishioka *et al.* [31] and Ohnishi *et al.* [32]. In the present work we have, for the first time, extended the application of this same three-body cluster model to the treatment of $(d,{}^6\mathrm{Li})$ within the CCBA. The ^{6}Li ground state and seven $d+\alpha$ continuum configurations, each of a given spin I and relative orbital angular momentum l ($l\leq 2$), are included in finite-range CCBA calculations. As with the elastic-scattering analyses, the coupling and diagonal channel interactions are generated consistently from the $d+\alpha$ cluster model.

The $d+\alpha$ continuum influences the $(d,{}^6\mathrm{Li})$ reaction in two ways. First, as with ^{6}Li elastic scattering, coupling to these states strongly affects the $^6\mathrm{Li}$-$^{60}\mathrm{Ni}$ channel distortion. Second, α transfers forming excited states of ^{6}Li provide alternate paths to the final state. Effective interactions, obtained from fits to ^{6}Li elastic scattering, have often been employed to simulate the effects of coupling to the ^{6}Li excited states. Because these interactions reproduce elastic scattering, they give a reasonable account of the channel wave functions in the extreme nuclear surface and beyond. They cannot however account for the effects of the different transfer paths. Consider the following two CCBA calculations. In the first we allow transfers into all eight ^{6}Li configurations while in the second we permit only the transfer leading directly to the ground state. Both calculations treat final-state distortion effects identically by allowing for coupling among all eight $d+\alpha$ states. Interference effects, introduced when the additional transfer paths are included, reduce the magnitude of the ground-state-transfer cross section by more than a factor of 2, yield predominantly positive values of A_y, rather than symmetric oscillations about zero, and alter A_{xx} and A_{yy} significantly. This result highlights the inappropriateness of ground-state–to–ground-state DWBA calculations based on optical potentials derived from ^{6}Li elastic scattering for predicting $(d,{}^6\mathrm{Li})$ observables.

Having concluded this, we have seen that, at the energies of the present work, application of the cluster model suffers considerable ambiguity. In particular, because of the low energies of the deuteron and α-particle clusters in the final state (5 and 10 MeV, respectively) one must estimate the underlying cluster-target interactions by extrapolating global potential parametrizations obtained from fitting higher-energy data. Detailed conclusions regarding the reaction mechanism at such energies, near the Coulomb barrier, are therefore difficult to make. Our calculations do show very clearly, however, the need to incorporate the low-lying $d+\alpha$ resonance states in any realistic analysis of the $(d,{}^6\mathrm{Li})$ reaction, be it for structure or spectroscopic purposes. Our difficulty in reproducing the data satisfactorily within the CCBA calculations may imply that other reaction processes, in addition to coupling via nuclear interactions to continuum $d+\alpha$ configurations, play an important role. No account has been taken, for instance, of possible Coulomb breakup contributions. At higher energies, Coulomb breakup is much less important, and the required cluster-target interactions are well determined. Hence, we believe that a CCBA analysis of existing high-energy data and the acquisition of additional, reasonably complete high-energy data sets would clarify the situation considerably.

ACKNOWLEDGMENTS

The authors wish to thank D. J. Abbott, C. M. Bhat, R. E. Fauber, T. M. Mooney, K. E. Nash, and T. C. Spencer for their assistance in acquiring the data and I. J. Thompson and R. L. Varner for their help in installing FRESCO at TUNL. This work was partially supported by the U.S. Department of Energy, Office of High Energy and Nuclear Physics, under Contract No. DE-AS05-76ER02408.

[1] I. J. Thompson, Comput. Phys. Commun. **7**, 167 (1988).
[2] J. Cook, Nucl. Phys. **A417**, 477 (1984).
[3] K. Umeda, T. Yamaya, T. Suehiro, K. Takimoto, R. Wada, E. Takada, S. Shimoura, A. Sakaguchi, S. Murakami, M. Fukada, and Y. Okuma, Nucl. Phys. **A429**, 88 (1984).
[4] J. Janecke, F. D. Becchetti, and D. Overway, Nucl. Phys. **A343**, 161 (1980).
[5] H. W. Fulbright, Annu. Rev. Nucl. Part. Sci. **29**, 161 (1979).
[6] W. Chung, J. van Hienen, B. H. Wildenthal, and C. L. Bennett, Phys. Lett. **79B**, 381 (1978).
[7] J. Cook and K. W. Kemper, Phys. Lett. **123B**, 5 (1983).
[8] G. Palla and W. Oelert, Phys. Rev. C **30**, 1331 (1984).
[9] W. W. Jacobs, E. J. Ludwig, J. E. Wilkerson, H. E. Conzett, P. Von Rossen, and R. M. Larimer, Bull. Am. Phys. Soc. **24**, 839 (1979).
[10] T. Yamaya, J. I. Hirota, K. Takimoto, S. Shimoura, A. Sakaguchi, S. Kubono, M. Sugitani, S. Kato, T. Suehiro, and M. Fukada, J. Phys. Soc. Jpn. Suppl. **55**, 730 (1986).
[11] T. Yamaya, T. Suehiro, S. Kato, J. I. Hirota, K. Takimoto, S. Shimoura, A. Sakagucchi, S. Kubono, M. Sugitani, and M. Fukada, J. Phys. Soc. Jpn. Suppl. **55**, 732 (1986).
[12] Y. Tagishi, Y. Aoki, M. Kurokawa, T. Murayama, T. Sakai, M. Takei, M. Tomizawa, and K. Yagi, Phys. Rev. C **35**, 1153 (1987).
[13] T. B. Clegg, G. A. Bissinger, and T. A. Trainor, Nucl. Instrum. Methods **120**, 445 (1974).
[14] H. W. Newson, E. G. Bilpuch, F. O. Purser, J. R. Boyce, and T. B. Clegg, Nucl. Instrum. Methods **122**, 99 (1974).
[15] J. E. Bowsher, Ph.D dissertation, University of North Carolina at Chapel Hill, 1989, available from University Microfilms International, 300 N. Zeeb Road, Ann Arbor, MI 48106.
[16] W. Haeberli, Annu. Rev. Nucl. Sci. **17**, 373 (1967).
[17] S. Tonsfeldt, Ph.D. dissertation, University of North Carolina at Chapel Hill, 1980, available from University Microfilms International, 300 N. Zeeb Road, Ann Arbor, MI 48106.
[18] G. G. Ohlsen and P. W. Keaton, Jr., Nucl. Instrum. Methods **109**, 41 (1973).
[19] M. H. MacFarlane and S. C. Pieper, Argonne National Laboratory Report ANL-76-11 Rev. 1 (unpublished); revised by R. P. Goddard, 1980 (unpublished).
[20] W. W. Daehnick, J. D. Childs, and Z. Vrcelj, Phys. Rev. C **21**, 2253 (1980).
[21] J. Cook, Nucl. Phys. **A388**, 153 (1982).
[22] D. R. Lehman and W. C. Parke, Phys. Rev. C **31**, 1920 (1985).
[23] H. Nishioka, J. A. Tostevin, and R. C. Johnson, Phys. Lett. **124B**, 17 (1983).
[24] K. I. Kubo and M. Hirata, Nucl. Phys. **A187**, 186 (1972).
[25] W. C. Parke and D. R. Lehman, Phys. Rev. C **29**, 2319 (1984).
[26] R. Ent, H. P. Block, J. F. A. van Hienen, G. van der Steenhoven, J. F. J. van den Brand, J. W. A. den Herder, E. Jans, P. H. M. Keizer, L. Lapikas, E. N. M. Quint, P. K. A. de W. Huberts, B. L. Berman, W. J. Briscoe, C. T. Christou, D. R. Lehman, B. E. Norum, and A. Saha, Phys. Rev. Lett. **57**, 2367 (1986).
[27] B. Jenny, W. Grüebler, V. Konig, P. A. Schmelzbach, and C. Schweizer, Nucl. Phys. **A397**, 61 (1983).
[28] Y. Sakuragi, Phys. Rev. C **35**, 2161 (1987).
[29] Y. Sakuragi, M. Yahiro, and M. Kamimura, Prog. Theor. Phys. Suppl. **89**, 136 (1986).
[30] J. Gomez-Camacho, M. Lozano, and M. A. Nagarajan, Phys. Lett. **161B**, 39 (1985).
[31] H. Nishioka, J. A. Tostevin, R. C. Johnson, and K. I. Kubo, Nucl. Phys. **A415**, 230 (1984).
[32] H. Ohnishi, M. Tanifuji, M. Kamimura, Y. Sakuragi, and M. Yahiro, Nucl. Phys. **A415**, 271 (1984).
[33] H. Nishioka, R. C. Johnson, J. A. Tostevin, and K. I. Kubo, Phys. Rev. Lett. **48**, 1795 (1982).
[34] A. Budzanowski, H. Dabrowski, L. Freindl, K. Grotowski, S. Micek, R. Planeta, A. Strzalkowski, M. Bosman, P. Leleux, P. Macq, J. P. Meulders, and C. Pirart, Phys. Rev. C **17**, 951 (1978).
[35] F. Ajzenberg-Selove, Nucl. Phys. **A490**, 1 (1988).
[36] P. A. Schmelzbach, W. Grüebler, V. Konig, and P. Marmier, Nucl. Phys. **A184**, 193 (1972).
[37] G. R. Satchler, *Direct Nuclear Reactions* (Oxford University Press, New York, 1983).
[38] D. A. Goldberg, S. M. Smith, and G. F. Burdzik, Phys. Rev. C **10**, 1362 (1974).
[39] I. J. Thompson and M. A. Nagarajan, Phys. Lett. **106B**, 163 (1981).
[40] W. Trombik, K. A. Eberhard, G. Hinderer, H. H. Rossner, A. Weidinger, and J. S. Eck, Phys. Rev. C **9**, 1813 (1974).

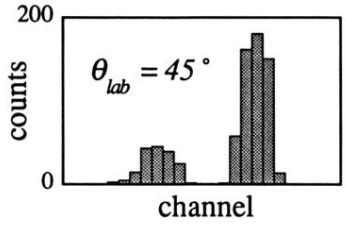

FIG. 1. Energy spectrum at $\theta_{lab}=45°$. The larger and smaller peaks correspond to $^{64}Zn(\vec{d},^{6}Li)$ forming the ground and first-excited states of ^{60}Ni, respectively.